THE JOURNAL OF PHYSICAL CHEMISTRY LETTERS
A JOURNAL OF THE AMERICAN CHEMICAL SOCIETY

pubs.acs.org/JPCL

Letter

Soliton Based Dynamic Nuclear Polarization: An Overhauser Effect in Cyclic Polyacetylene at High Field and Room Temperature

Z. Miao, F. J. Scott, J. van Tol, C. R. Bowers, A. S. Veige, and F. Mentink-Vigier*

Cite This: *J. Phys. Chem. Lett.* 2024, 15, 3369−3375

Read Online

ACCESS | Metrics & More | Article Recommendations | Supporting Information

ABSTRACT: Polyacetylene, a versatile material with an electrical conductivity that can span 7 orders of magnitude, is the prototypical conductive polymer. In this letter, we report the observation of a significant Overhauser effect at the high magnetic field of 14.1 T that operates at 100 K and room temperature in both linear and cyclic polyacetylene. Significant NMR signal enhancements ranging from 24 to 45 are obtained. The increased sensitivity enabled the characterization of the polymer chain defects at natural abundance. The absence of end methyl group carbon-13 signals provides proof of the closed-loop molecular structure of cyclic polyacetylene. The remarkable efficiency of the soliton based Overhauser effect DNP mechanism at high temperature and high field holds promise for applications and extension to other conductive polymer systems.

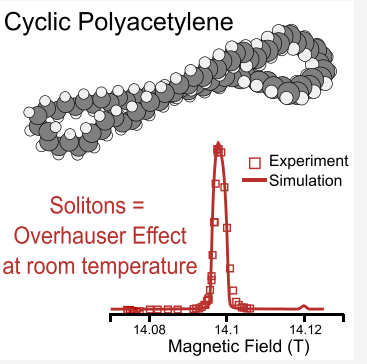

In recent years, the research and utilization of conductive polymers has expanded significantly, with applications ranging from optoelectronics to materials science.[1] Linear polyacetylene (linear PA), the simplest polyene and the most extensively studied organic conjugated polymer, was first synthesized using titanium-based catalysts by Natta et al. in 1958.[2] A major breakthrough occurred when Shirakawa et al. synthesized free-standing films of linear PA, endowing PA materials with both mechanical flexibility as a polymer film[3,4] and, after doping, conductivities comparable to metals at room temperature.[5,6] When synthesized at −78 °C using Shirakawa et al.'s method, linear PA contains *cis* double bonds as a natural consequence of an insertion mechanism[2] but the more stable *trans*−*transoid* isomer with higher conductivities can be obtained via thermal isomerization.[3,7] In 2021, we reported the synthesis of cyclic polyacetylene (cyclic PA; Figure 2).[8−10] Unique to its topology, cyclic PA synthesized with catalyst **1**[11−15] (Scheme 1) exhibits an exclusively *trans*−*transoid* structure, even when synthesized at −94 °C.[9]

Characterizing polyacetylene is a challenge because it is insoluble. For such materials, solid-state NMR provides unrivaled structural information on the atomic scale. However, conventional solid-state NMR is a notoriously insensitive technique, which makes it challenging to detect chemical sites at low concentrations. The sensitivity of solid-state NMR can be increased by combining magic angle spinning (MAS) with dynamic nuclear polarization (DNP). DNP increases the nuclear spin polarization via irradiation of electron spin resonance transitions associated with paramagnetic centers with a high power microwave (μw) source.[16−21] With only a few notable exceptions,[22−24] MAS-DNP in high magnetic fields

Scheme 1. Synthesis of Cyclic Polyacetylene with Catalyst 1[a]

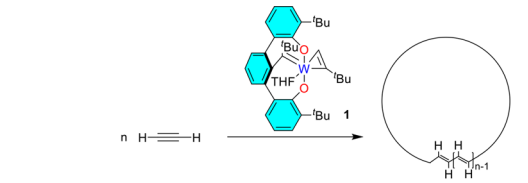

[a]Panels A−C depicts various samples of cyclic polyacetylene that can be produced with catalyst **1**.

is carried out with extrinsic paramagnetic species at low temperature where the electron and nuclear spin dynamics is more favorable.[25−27] DNP using intrinsic paramagnetic species is interesting as it directly probes the properties, spin interactions, and spin dynamics of the material itself.[28−30] In

Received: December 23, 2023
Revised: March 8, 2024
Accepted: March 11, 2024
Published: March 18, 2024

https://doi.org/10.1021/acs.jpclett.3c03591
J. Phys. Chem. Lett. 2024, 15, 3369−3375

this context, conductive polymers are intriguing materials for fundamental studies of high-field MAS-DNP that can serve as a unique probe of structure and dynamics in solids with extended electronic states. Among conductive polymers, linear PA is known to display efficient Overhauser effect (OE) DNP at low fields ranging from 0.3 to 1.4 T using the bond alternation domain wall (i.e. solitons[31]) and trapped unpaired electron spins.[32−35] However, DNP on conductive samples at high field is challenging. It requires the sample to be sufficiently transparent to the μw irradiation, but since the skin depth in conductors is inversely proportional to the frequency, the volume that is effectively irradiated is limited, and μw absorption can result in significant sample heating, even for materials with modest conductivity.[36] In addition, the dynamic properties of the spin system, particularly the spectral density of the fluctuations in the electron−nuclear coupling at the Larmor frequency difference, need to be sufficient to generate DNP at high field, which is one of the key challenges of OE in liquids.[37,38] Therefore, reports of room temperature MAS-DNP in paramagnetic organic materials at high field are rare, and to our knowledge, DNP in a conductive organic solid at high magnetic field ($\geq$14.1 T) has not been previously reported.

In this letter we report strong ^{1}H MAS-DNP signal enhancements ranging between 24 and 45 in both undoped linear and cyclic polyacetylene (*trans*−*transoid*),[39] hereafter referred to as linear PA and cyclic PA, at high field and room temperature. The explanation of the origin of these remarkable signal enhancements is guided by previous studies on linear PA[32−35] together with EPR spectroscopy and numerical simulations based on the Overhauser (OE) and solid effect (SE) mechanisms. These large enhancements enabled us to analyze the topological and chemical defects in the novel cyclic conductive polymer.[39] The quality of the data suggests that the method is extensible to other conductive polymers.[1,40]

Conductive polymers such as polyacetylene contain defects in the π-conjugation that are referred to as bond alternation domain-walls or solitons[31] that bear isolated unpaired electrons.[40] The conduction mechanism is different from that in metals as it relies on the presence of these electronic defects with energy levels in the band gap as in semiconductors. Here, the linear and cyclic PA samples were initially characterized by EPR. The room temperature X-band EPR spectra (9.6 GHz/0.3 T) presented in Figure S1 of the Supporting Information exhibit a single, featureless resonance reflecting the high mobility of the conduction electrons which averages the local spin interactions,[41,42] i.e., the g-tensor and hyperfine couplings. The EPR line width is 0.12 mT for the linear PA (similar to previous reports)[32] and 0.2 mT for cyclic PA. The motional narrowing indicates that the correlation time is much shorter than the inverse of the largest hyperfine coupling, $\frac{1}{|A|_{max}} \approx \frac{1}{12\ \text{MHz}}$ [42] with an upper bound of $\sim 10^{-13}$ s,[32,33,35,43] consistent with the literature reports for linear PA.[33,41] The high-field EPR spectra at 8.4 T/240 GHz at a series of different temperatures are presented in Figure 1. In both samples, the EPR transition broadens as the temperature is reduced from 220 to 10 K. At this field, the low temperature EPR line widths at 100 K are 1.64 mT and 1.27 mT, respectively, considerably larger than at X-band.[32] At high field, the effect of g-tensor anisotropy on the EPR spectra is more important and motional narrowing is not as effective. Fits of the EPR spectra for both samples at 100 and 10 K using a single spin population are

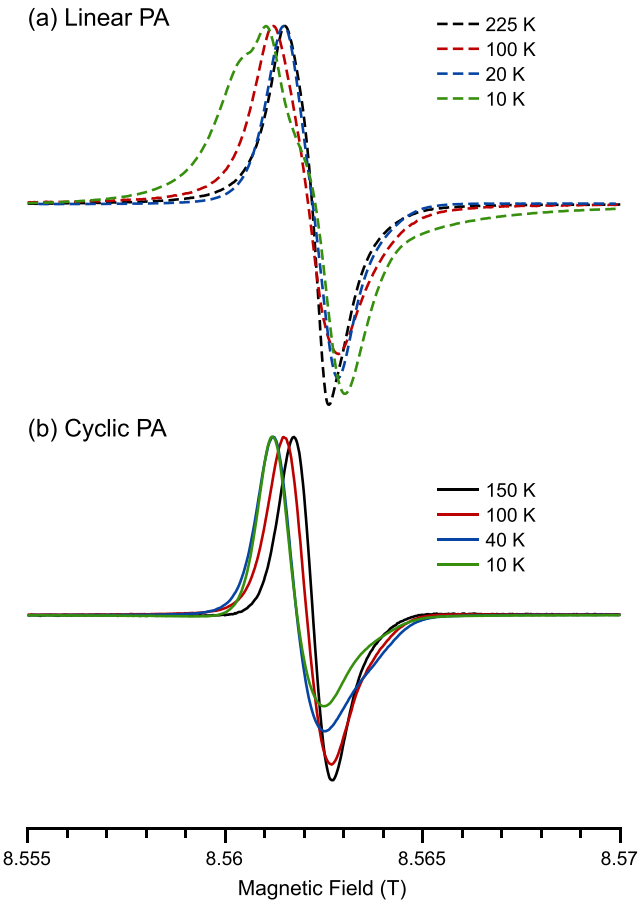

Figure 1. EPR spectra as a function of temperature of (a) linear PA and (b) cyclic PA collected between 225 and 10 K at 240 GHz.

reported in Figure S5. While at 100 K the agreement is reasonable, it is poor at 10 K, especially for the linear PA. The EPR spectra of the linear PA sample exhibit additional features at 10 K, as does the cyclic PA to a lesser extent. This observation aligns with the existing literature, suggesting the presence of two distinct spin populations in linear PA: one comprised of delocalized electron spins that move along the chain and another consisting of electrons trapped in localized defects.[32,33,35,40,44] As the temperature decreases, the delocalized electrons become trapped within the defect sites, leading to reduced motional narrowing.[32,33,41,42,44] In linear PA, the exact nature of the defect sites is debated; they could arise from either O_2 exposure[32,33] or residual *cis* bonds.[43] The soliton mobility in cyclic PA follows the same trend. The EPR line exhibits some asymmetry as the temperature is decreased, also indicating reduced motional narrowing. However, at 10 K the EPR line width of cyclic PA is only half of that of the linear PA EPR spectrum and presents fewer features. This suggests that the reduction in the mobility within cyclic PA is less pronounced. This is consistent with a lower density of topological (e.g., *cis* bonds) and polymer chain defects in the cyclic PA sample and/or a soliton trapping potential that is shallower compared to that of the linear PA sample.[32,35,45]

MAS-DNP NMR experiments were performed on linear and cyclic PA samples at magnetic fields of around 14.1 T or 600 MHz ^{1}H Larmor frequency. Figure 2a presents plots of the ^{1}H NMR signal enhancements as a function of the static magnetic field for a fixed μw frequency of 395.145 GHz at 100 K. Both samples exhibit maximum enhancement of the ^{1}H nuclear spin

https://doi.org/10.1021/acs.jpclett.3c03591
J. Phys. Chem. Lett. 2024, 15, 3369−3375

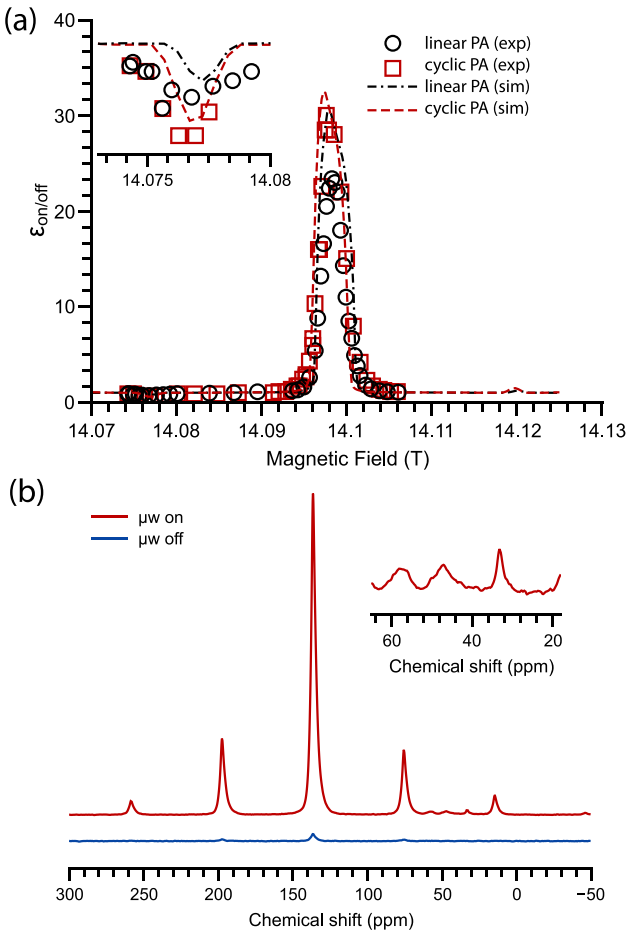

Figure 2. (a) ^{1}H MAS-DNP field profiles for linear PA (black circles) and cyclic PA (red squares, sample 2) collected at 100 K and 9.2 kHz spinning speed and the corresponding simulated enhancement using the two-spin model (dashed line, same colors) of eq 2. The inset is a focused view of the solid-effect negative (DQ) enhancement region. (b) ^{1}H → ^{13}C CP spectra of cyclic PA (sample 1) collected at room temperature with (red) and without (blue) μw irradiation (19 W, see Supporting Information). A focused view of the cyclic PA polymer chemical defect region is displayed in the inset.

polarization for μw irradiation under the EPR resonance condition. Significant enhancements of 24 and 32 were obtained for linear PA and cyclic PA, respectively. In addition, a modest nuclear spin depolarization is observed at the lower field of 14.078 T. The sign of the enhancement remains constant in the vicinity of ∼14.095 T which is characteristic of the Overhauser effect (OE) mechanism.[46−48] In addition, the maximum enhancement is obtained for a modest μw irradiation strength (∼8 W at 100 K; see Figure S2) while the depolarization at ∼14.078 T is attributed to the SE[49,50] mechanism where irradiation of the double quantum electron−nucleus transition generates a polarization below thermal equilibrium.

As seen in Figure 2a, the enhancement due to the OE in cyclic PA is significantly larger than the SE enhancement, as it reaches 32 while for the SE it is only ∼0.6. For the linear PA sample, the OE enhancement is as high as 24 but only 0.7 for the SE condition. The observation of the OE indicates a fast fluctuation of the isotropic hyperfine couplings with an upper limit on the correlation time of $1/(2\pi \times 395\ \text{GHz}) \approx 4.10^{-13}$ s that can be attributed to the soliton dynamics.[32,35,51]

Nevertheless, the identification of the SE DNP mechanism implies that the anisotropic hyperfine coupling is not entirely averaged at 100 K. Again, this suggests that either the motional averaging resulting from electron spin delocalization is incomplete or there are two distinct populations of unpaired electron spins. The former assertion aligns with experimental findings in linear PA[32,33,35,44,52] as well as the high field EPR spectra. Hence, it is reasonable to extend this interpretation to cyclic PA. Since the two electron spin populations have identical Larmor frequencies, the enhancement field profile was simulated by considering the coupling between N nuclear spins and n electron spins split into two populations, n_1 on site #1 and n_2 on site #2. The coupling for both should be temperature dependent. The corresponding rotating frame spin Hamiltonian is given by

$$\hat{H}_0 = \sum_{l=1}^{n} ((g\beta B_0 - \Delta\omega)\hat{S}_{z,l} + \omega_1 \hat{S}_{x,l} + \sum_{k=1}^{N} \left(\sum_{l=1}^{n_1} A^{\text{iso}}_{z,l,k} \hat{S}_{z,l} \hat{I}_{z,k} + \sum_{m=1}^{n_2} +2A^{\text{aniso}}_{z,m,k} \hat{S}_{z,m} \hat{I}_{z,k} + A^{\text{aniso}}_{+,m,k} \hat{S}_{z,m} \hat{I}_{+,k} + A^{\text{aniso}}_{-,m,k} \hat{S}_{z,m} \hat{I}_{-,k} \right) \quad (1)$$

The first two terms relate to the Zeeman and μw interactions, while the remaining terms represent the hyperfine couplings to the nuclei. We assume that the nuclei are equilibrating quickly and, thus, can be represented as a single nucleus. Since the two mechanisms are well separated in frequency, the problem can be reduced to a simple "two-spin" system where only the "average" hyperfine couplings are considered for each of the two populations:

$$\hat{H}_0 = (g\beta B_0 - \Delta\omega)\hat{S}_z + \omega_1 \hat{S}_x + \hat{S}_z(\langle 2A^{\text{iso}}_z + A^{\text{aniso}}_z \rangle \langle \hat{I}_z \rangle + \langle A^{\text{aniso}}_+ \rangle \langle \hat{I}_+ \rangle + \langle A^{\text{aniso}}_- \rangle \langle \hat{I}_- \rangle) \quad (2)$$

Under this approach, $\langle A^{\text{iso}}_z \rangle$ and $\langle A^{\text{aniso}}_{z/\pm} \rangle$ should be temperature dependent as they depend on the relative site populations n_1 and n_2. The simulations of the field profile used the fitted g-values at 100 K and the measured intrinsic nuclear spin−lattice relaxation times (0.45 s for linear PA and 0.5 s for cyclic PA sample 2). From these relaxation times and DFT simulations reported in the Supporting Information, it is possible to extract the zero quantum (ZQ) and double quantum (DQ) relaxation rates, assuming a 1D diffusion of the solitons with a diffusion coefficient, $D_{\parallel}$.[32] The simulations of the OE and SE are reported in Figure 2a as dashed lines and the previously reported electron spin relaxation time for linear PA (0.1 ms).[35,52] The only fitting parameter is $\langle A^{\text{aniso}} \rangle$ that we found to be 0.2 MHz, to reach a good agreement with the SE enhancement. The agreement between experiments and simulations for the OE is very good for the cyclic PA and satisfactory for the linear PA. The maximum enhancement is well reproduced for the cyclic PA and slightly overestimated for the linear PA. The relaxation model previously developed[32,33] (see details in the Supporting Information) is thus robust and appears to be suitable for both samples.

The OE DNP mechanism was further explored by measuring the ^{13}C enhancement due to direct polarization (see Table 1). At 100 K, it is on the same order of magnitude as the ^{1}H enhancement. Nuclear spin diffusion between ^{13}C nuclei at natural isotopic abundance is negligible; hence, the

https://doi.org/10.1021/acs.jpclett.3c03591
J. Phys. Chem. Lett. 2024, 15, 3369−3375

Table 1. Measured Values of the ^{1}H and ^{13}C Polarization Enhancements $\epsilon_{on/off}$ and Build-up Times T_B for Linear PA and Cyclic PA[a]

	OE ^{1}H				OE ^{13}C (direct)	
	$\epsilon_{on/off}$		T_B (s)		max $\epsilon_{on/off}$	T_B (s)
sample	100 K	290 K	100 K	290 K	100 K	100 K
Linear PA	24	26	0.45	0.3	~20	32
Cyclic PA, sample 1	30	45	1	0.5	~30	90
Cyclic PA, sample 2	32	38	0.5	0.26	~48	

[a]Note that the build-up time for the ^{13}C sample is not purely monoexponential, and the reported T_B is the approximate time constant.

observed large enhancement values confirm that the solitons are well delocalized over the chains.

Previous publications in the 1980s on linear *trans*-PA reported proton polarization enhancements with OE DNP at room temperature. However, most of the experiments were carried out at low fields ($B_0 \leq 1.4$ T)[34,35,53,54] where conditions are much more favorable for DNP in a conductive material (*vide supra*) but resulted in low resolution NMR spectra. As reported in Table 1, we found that the DNP enhancement in cyclic PA at 100 K exceeds that of linear PA at 14.1 T, and furthermore, the enhancement in the former is even greater at room temperature (RT). This enhancement increased from ~30 at 100 K to 45 at RT for one of the samples tested. At RT, the buildup times are shorter, yet the enhancements are higher. The shortening of the nuclear relaxation times by a factor 2 can be explained by the relaxation models in a 1D chain that should follow the equation[32] $\frac{1}{T_{1,n}} \propto \frac{n_1(T)T}{\sqrt{D_\parallel}}$ (see Supporting Information). The increased enhancements at RT can be due to an increase in the number of spins that generates OE; in other words $n_1(T)$ increases and $n_2(T)$ decreases which in turn increases the number of nuclei that undergo OE. This further supports our hypothesis for the existence of two populations of solitons in cyclic PA: the mobile population that generates the OE is increased at high temperature and the trapped electron spin population, which generates the SE, is increased at low temperature as proposed previously for linear PA.[35] Predicting the OE signal enhancement at room temperature requires knowledge of (1) the electron spin relaxation times at the experimental magnetic field (14.1 T), (2) accurate measurements of the diffusion coefficient, $D_\parallel$, (3) the ratio $n_2(T)/n_1(T)$, and (4) the exact concentration $n_1(T) + n_2(T)$. Since accurate values for these parameters are unavailable, we are unable to predict these enhancements. This is discussed in more detail in the Supporting Information.

MAS-DNP experiments were repeated on multiple cyclic PA samples prepared and isomerized under various conditions. The observed enhancements all fell within the range of ~30–36 and T_B ranged from 0.25 to 0.5 s at room temperature (see Table S1). In Table 1 we report the results for two cyclic PA samples at RT and 100 K that led to the largest nuclear

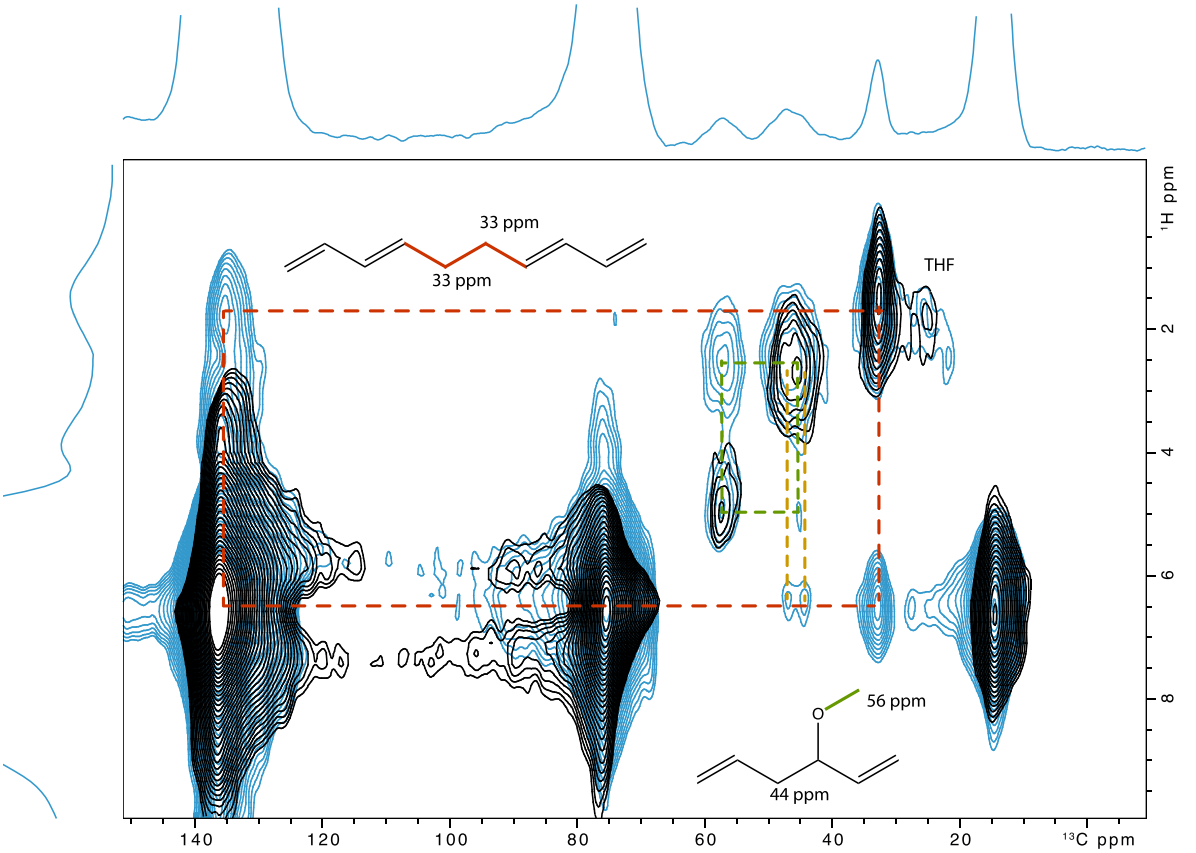

Figure 3. $^{1}H-^{13}C$ correlation spectrum for cyclic PA using two different cross-polarization contact times, 40 μs (black) and 400 μs (blue). Spectra were collected at 100 K and 9.2 kHz.

https://doi.org/10.1021/acs.jpclett.3c03591
J. Phys. Chem. Lett. 2024, 15, 3369−3375

polarization buildup time difference (0.5 s vs 1 s). This difference can be explained, in part, to different concentrations of conduction electrons (see Figure S2) but also to other factors yet to be determined.

Importantly, these significant enhancements enabled for the first time the collection of $^{1}H-^{13}C$ cross-polarization (CP)[55] spectra at both temperatures with very high sensitivity. The cyclic PA ^{13}C NMR spectra at room temperature, with and without μw irradiation (at the maximum OE position), are reported in Figure 2b. It is important to note the spectra at room temperature and 100 K are near identical (see Figure S4). Despite the higher enhancement at room temperature, the higher spin polarization, and the better signal-to-noise performance of the NMR probe, the sensitivity remains better at the lowest temperature. The combination of high magnetic field and high signal-to-noise enabled the recording of ^{13}C signals from defect sites in the 0 to ∼100 ppm chemical shift range on the neat samples. Previous low field DNP studies attempted to identify the chemical structure of defects of linear PA under oxidative condition, but the lack of resolution in that work made the assignment challenging.[34] Here we take advantage of the high resolution and very high sensitivity to address two key questions about these cyclic PA samples. First, can we confirm that the chains are indeed cyclic? Second, what defects are observed in the neat sample?

The 1D ^{13}C NMR spectrum is dominated by the $-\mathbf{C}H=\mathbf{C}H-$ signal at 136.5 ppm, originating from the main chain. However, resonances at 25, 33, 46, 48, and 56 ppm are also clearly visible and correspond to various types of "defects". Those defect signals are enhanced by the same amount as the main chain signals which indicates a close spatial proximity with the main polymers. These signals are confirmed by spectra at different MAS rates at 100 K and room temperature (see Supporting Information). These signals are different from those observed in linear PA (see Supporting Information). The presence of signals in the 15−20 ppm range, typically associated with $-CH_3$, is observed for the linear PA but not for the cyclic PA (see Figure S4). Such methyl groups are associated with chain termination,[34] and their absence is consistent with a closed cycle PA chain topology. The signal at ∼25/1.8 ppm ($^{13}C/^{1}H$ chemical shift) may correlate with the main chain but is more likely to be indicative of tetrahydrofuran solvent molecules that can remain trapped in the polymer after synthesis.

Assignment of additional signals based on the 1D spectra is not possible or at least ambiguous. Therefore, we took advantage of the high sensitivity to carry out $^{1}H-^{13}C$ correlation experiments with different CP times to assess the proximity of the sites to solitons. Figure 3 reports the correlations obtained using a contact time of 40 or 400 μs. In the first case, the spin diffusion among ^{1}H nuclear spins during CP is minimal, and thus, no long-range correlations are observed. For the longer CP time, the spin diffusion among proximal ^{1}H nuclear spins, enables probing of the chemical nature of the ^{1}H surrounding the ^{13}C sites. Based on this approach, the signals at 33 ppm (1.8−2 ppm in the ^{1}H frequency dimension) correlate with the main peak at 136.5 ppm. These carbons belong to the main chain, and their chemical shift indicates they are saturated sites $=CH-\mathbf{C}H_2-\mathbf{C}H_2-CH=$ as shown in Figure 3. The signals at 46 and 48 ppm correlate with the main signals at 136.5 ppm. This indicates that these carbons are close to the main chain. However, the lower cross peak intensity indicates that these sites are further away from the main chain. Finally, the peak at 56 ppm only correlates with the signal at 46 ppm but not the main chain. This site is thus even further away from the main chain as it does not correlate with it. Based on the chemical shifts, these sites could be $\mathbf{C}H_3-O-$ that are connected to the main chain via an unsaturated site $-\mathbf{C}H-$ resonating at 46 ppm. Such a site would be the result of partial oxidation on the sample's surface. It is nonetheless difficult to attribute the signal with full confidence.

In summary, this study establishes the feasibility of DNP on conductive polymers at very high magnetic fields, utilizing solitons as a nuclear hyperpolarization source. The experiments, performed on linear PA and the recently synthesized cyclic PA, revealed a remarkable enhancement that is attributed to the Overhauser effect originating from the solitons, which intriguingly persists even at room temperature where an enhancement factor of 45 was reached, a record for intrinsic defects under such high magnetic field.

The combination of enhanced sensitivity and high resolution was instrumental in determining the structural composition of the defects in cyclic PA. Notably, the absence of methyl groups within the cyclic PA is unveiled, further confirming its inherent cyclic nature and excluding the presence of detectable linear chains. This achievement not only advances our understanding of cyclic PA but also establishes a pathway toward the comprehensive analysis of conductive polymers, which are pivotal components in the landscape of molecular electronics and optoelectronics.[1]

■ ASSOCIATED CONTENT

Supporting Information

The Supporting Information is available free of charge at https://pubs.acs.org/doi/10.1021/acs.jpclett.3c03591.

Experimental details and associated content (PDF)

■ AUTHOR INFORMATION

Corresponding Author

F. Mentink-Vigier − *National High Magnetic Field Laboratory, Florida State University, Tallahassee, Florida 32310, United States;* orcid.org/0000-0002-3570-9787; Email: fmentink@magnet.fsu.edu

Authors

Z. Miao − *Center for Catalysis, Department of Chemistry, University of Florida, Gainesville, Florida 32611, United States*

F. J. Scott − *National High Magnetic Field Laboratory, Florida State University, Tallahassee, Florida 32310, United States;* orcid.org/0000-0003-3903-8842

J. van Tol − *National High Magnetic Field Laboratory, Florida State University, Tallahassee, Florida 32310, United States;* orcid.org/0000-0001-6972-2149

C. R. Bowers − *Center for Catalysis, Department of Chemistry, University of Florida, Gainesville, Florida 32611, United States; National High Magnetic Field Laboratory, Florida State University, Tallahassee, Florida 32310, United States;* orcid.org/0000-0001-6155-5163

A. S. Veige − *Center for Catalysis, Department of Chemistry, University of Florida, Gainesville, Florida 32611, United States;* orcid.org/0000-0002-7020-9251

Complete contact information is available at: https://pubs.acs.org/10.1021/acs.jpclett.3c03591

https://doi.org/10.1021/acs.jpclett.3c03591
J. Phys. Chem. Lett. 2024, 15, 3369−3375

Notes

The authors declare no competing financial interest.

■ ACKNOWLEDGMENTS

The National High Magnetic Field Laboratory (NHMFL) is funded by the National Science Foundation Division of Materials Research (Grants DMR-1644779 and DMR-2128556) and the State of Florida. A portion of this work was supported by Grant NIH RM1-GM148766 and the European Union's Horizon 2020 Research and Innovation Programme under Grant Agreement No. 101008500. F.J.S. acknowledges support from a Diversity Postdoctoral Scholar award from the Provost's Office at Florida State University. C.R.B. acknowledges support from NSF Grants CHE-2108306 and CBET-1933723. A.S.V. acknowledges support from NSF Grant CHE-2108266.

■ REFERENCES

(1) Nezakati, T.; Seifalian, A.; Tan, A.; Seifalian, A. M. Conductive Polymers: Opportunities and Challenges in Biomedical Applications. *Chem. Rev.* **2018**, *118*, 6766−6843.
(2) Natta, G.; Mazzanti, G.; Corradini, P. *Atti Acad. Naz. Lincei, Cl. Sci. Fis. Mat. Nat., Rend.* **1958**, *25*, 3.
(3) Ito, T.; Shirakawa, H.; Ikeda, S. Simultaneous polymerization and formation of polyacetylene film on the surface of concentrated soluble Ziegler-type catalyst solution. *J. Polym. Sci. Polym. Chem. Ed.* **1974**, *12*, 11−20.
(4) Shirakawa, H.; Ikeda, S. Infrared Spectra of Poly(acetylene). *Polym. J.* **1971**, *2*, 231−244.
(5) Shirakawa, H.; Louis, E. J.; MacDiarmid, A. G.; Chiang, C. K.; Heeger, A. J. Synthesis of electrically conducting organic polymers: halogen derivatives of polyacetylene, (CH)x. *J. Chem. Soc., Chem. Commun.* **1977**, 578.
(6) Chiang, C. K.; Fincher, C. R.; Park, Y. W.; Heeger, A. J.; Shirakawa, H.; Louis, E. J.; Gau, S. C.; MacDiarmid, A. G. Electrical Conductivity in Doped Polyacetylene. *Phys. Rev. Lett.* **1977**, *39*, 1098−1101.
(7) Chien, J. C. W.; Karasz, F. E.; Wnek, G. E. Soliton formation and cis trans isomerization in polyacetylene. *Nature* **1980**, *285*, 390−392.
(8) Miao, Z.; Gonsales, S. A.; Ehm, C.; Mentink-Vigier, F.; Bowers, C. R.; Sumerlin, B. S.; Veige, A. S. Cyclic polyacetylene. *Nat. Chem.* **2021**, *13*, 792−799.
(9) Miao, Z.; Esper, A. M.; Nadif, S. S.; Gonsales, S. A.; Sumerlin, B. S.; Veige, A. S. Semi-conducting cyclic copolymers of acetylene and propyne. *React. Funct. Polym.* **2021**, *169*, No. 105088.
(10) Miao, Z.; Konar, D.; Sumerlin, B. S.; Veige, A. S. Soluble Polymer Precursors via Ring-Expansion Metathesis Polymerization for the Synthesis of Cyclic Polyacetylene. *Macromolecules* **2021**, *54*, 7840−7848.
(11) Jakhar, V. K.; Shen, Y.-H.; Hyun, S.-M.; Esper, A. M.; Ghiviriga, I.; Abboud, K. A.; Lester, D. W.; Veige, A. S. Improved Trianionic Pincer Ligand Synthesis for Cyclic Polymer Catalysts. *Organometallics* **2023**, *42*, 1339−1346.
(12) Kuppuswamy, S.; Peloquin, A. J.; Ghiviriga, I.; Abboud, K. A.; Veige, A. S. Synthesis and Characterization of Tungsten(VI) Alkylidene Complexes Supported by an $[OCO]^{3-}$ Trianionic Pincer Ligand: Progress towards the $[^{t}BuOCO]W{\equiv}CC(CH_3)_3$ Fragment. *Organometallics* **2010**, *29*, 4227−4233.
(13) McGowan, K. P.; O'Reilly, M. E.; Ghiviriga, I.; Abboud, K. A.; Veige, A. S. Compelling mechanistic data and identification of the active species in tungsten-catalyzed alkyne polymerizations: conversion of a trianionic pincer into a new tetraanionic pincer-type ligand. *Chem. Sci.* **2013**, *4*, 1145−1155.
(14) Roland, C. D.; Li, H.; Abboud, K. A.; Wagener, K. B.; Veige, A. S. Cyclic polymers from alkynes. *Nature Chem.* **2016**, *8*, 791−796.
(15) Sarkar, S.; McGowan, K. P.; Kuppuswamy, S.; Ghiviriga, I.; Abboud, K. A.; Veige, A. S. An OCO^{3-} Trianionic Pincer Tungsten(VI) Alkylidyne: Rational Design of a Highly Active Alkyne Polymerization Catalyst. *J. Am. Chem. Soc.* **2012**, *134*, 4509−4512.
(16) Lilly Thankamony, A. S.; Wittmann, J. J.; Kaushik, M.; Corzilius, B. Dynamic nuclear polarization for sensitivity enhancement in modern solid-state NMR. *Prog. Nucl. Magn. Reson. Spectrosc.* **2017**, *102*−*103*, 120−195.
(17) Rankin, A. G. M.; Trébosc, J.; Pourpoint, F.; Amoureux, J.-P.; Lafon, O. Recent developments in MAS DNP-NMR of materials. *Solid State Nucl. Magn. Reson.* **2019**, *101*, 116−143.
(18) Lee, D.; Hediger, S.; De Paëpe, G. Is solid-state NMR enhanced by dynamic nuclear polarization? *Solid State Nucl. Magn. Reson.* **2015**, *66*−*67*, 6−20.
(19) Reif, B.; Ashbrook, S. E.; Emsley, L.; Hong, M. Solid-state NMR spectroscopy. *Nat. Rev. Methods Primers* **2021**, *1*, 2.
(20) Rossini, A. J.; Zagdoun, A.; Lelli, M.; Lesage, A.; Coperet, C.; Emsley, L. Dynamic nuclear polarization surface enhanced NMR spectroscopy. *Accounts of chemical research* **2013**, *46*, 1942−51.
(21) Maly, T.; Debelouchina, G. T.; Bajaj, V. S.; Hu, K.-N.; Joo, C.-G.; Mak-Jurkauskas, M. L.; Sirigiri, J. R.; van der Wel, P. C. A.; Herzfeld, J.; Temkin, R. J.; Griffin, R. G. Dynamic nuclear polarization at high magnetic fields. *J. Chem. Phys.* **2008**, *128*, No. 052211.
(22) Hope, M. A.; Rinkel, B. L. D.; Gunnarsdóttir, A. B.; Märker, K.; Menkin, S.; Paul, S.; Sergeyev, I. V.; Grey, C. P. Selective NMR observation of the SEI−metal interface by dynamic nuclear polarisation from lithium metal. *Nat. Commun.* **2020**, *11*, 2224.
(23) Lelli, M.; Chaudhari, S. R.; Gajan, D.; Casano, G.; Rossini, A. J.; Ouari, O.; Tordo, P.; Lesage, A.; Emsley, L. Solid-State Dynamic Nuclear Polarization at 9.4 and 18.8 T from 100 K to Room Temperature. *J. Am. Chem. Soc.* **2015**, *137*, 14558−14561.
(24) Hope, M. A.; Björgvinsdóttir, S.; Halat, D. M.; Menzildjian, G.; Wang, Z.; Zhang, B.; MacManus-Driscoll, J. L.; Lesage, A.; Lelli, M.; Emsley, L.; Grey, C. P. Endogenous ^{17}O Dynamic Nuclear Polarization of Gd-Doped CeO_2 from 100 to 370 K. *J. Phys. Chem. C* **2021**, *125*, 18799−18809.
(25) Hall, D. A.; Maus, D. C.; Gerfen, G. J.; Inati, S. J.; Becerra, L. R.; Dahlquist, F. W.; Griffin, R. G. Polarization-Enhanced NMR Spectroscopy of Biomolecules in Frozen Solution. *Science* **1997**, *276*, 930−932.
(26) Thurber, K. R.; Tycko, R. Theory for cross effect dynamic nuclear polarization under magic-angle spinning in solid state nuclear magnetic resonance: the importance of level crossings. *J. Chem. Phys.* **2012**, *137*, No. 084508.
(27) Mentink-Vigier, F.; Akbey, U.; Hovav, Y.; Vega, S.; Oschkinat, H.; Feintuch, A. Fast passage dynamic nuclear polarization on rotating solids. *J. Magn. Reson.* **2012**, *224*, 13−21.
(28) DeHaven, B. A.; Tokarski, J. T.; Korous, A. A.; Mentink-Vigier, F.; Makris, T. M.; Brugh, A. M.; Forbes, M. D. E.; van Tol, J.; Bowers, C. R.; Shimizu, L. S. Persistent Radicals of Self-assembled Benzophenone *bis* -Urea Macrocycles: Characterization and Application as a Polarizing Agent for Solid-state DNP MAS Spectroscopy. *Chem.—Eur. J.* **2017**, *23*, 8315−8319.
(29) Harchol, A.; Reuveni, G.; Ri, V.; Thomas, B.; Carmieli, R.; Herber, R. H.; Kim, C.; Leskes, M. Endogenous Dynamic Nuclear Polarization for Sensitivity Enhancement in Solid-State NMR of Electrode Materials. *J. Phys. Chem. C* **2020**, *124*, 7082−7090.
(30) Carnahan, S. L.; Chen, Y.; Wishart, J. F.; Lubach, J. W.; Rossini, A. J. Magic angle spinning dynamic nuclear polarization solid-state NMR spectroscopy of γ-irradiated molecular organic solids. *Solid State Nucl. Magn. Reson.* **2022**, *119*, No. 101785.
(31) Su, W. P.; Schrieffer, J. R.; Heeger, A. J. Soliton excitations in polyacetylene. *Phys. Rev. B* **1980**, *22*, 2099−2111.
(32) Nechtschein, M.; Devreux, F.; Genoud, F.; Guglielmi, M.; Holczer, K. Magnetic-resonance studies in undoped trans-polyacetylene CH_x. II. *Phys. Rev. B* **1983**, *27*, 61−78.
(33) Holczer, K.; Boucher, J. P.; Devreux, F.; Nechtschein, M. Magnetic-resonance studies in undoped trans-polyacetylene, CH_x. *Phys. Rev. B* **1981**, *23*, 1051−1063.
(34) Wind, R. A.; Duijvestijn, M. J.; Vriend, J. Structural defects in undoped trans-polyacetylene, before and after air oxidation, studied

https://doi.org/10.1021/acs.jpclett.3c03591
J. Phys. Chem. Lett. 2024, 15, 3369−3375

by DNP-enhanced 13C NMR. *Solid State Commun.* **1985**, *56*, 713−716.
(35) Clark, W. G.; Glover, K.; Mozurkewich, G.; Etemad, S.; Maxfield, M. Measurements of Soliton Trapping and Motion in Trans-Polyacetylene Using Dynamic Nuclear Polarization. *Mol. Cryst. Liq. Cryst.* **1985**, *117*, 447−454.
(36) Svirinovsky-Arbeli, A.; Rosenberg, D.; Krotkov, D.; Damari, R.; Kundu, K.; Feintuch, A.; Houben, L.; Fleischer, S.; Leskes, M. The effects of sample conductivity on the efficacy of dynamic nuclear polarization for sensitivity enhancement in solid state NMR spectroscopy. *Solid State Nucl. Magn. Reson.* **2019**, *99*, 7−14.
(37) Denysenkov, V. P.; Prisner, T. F. In *eMagRes*; John Wiley & Sons, Ltd., 2019; pp 41−54.
(38) Bennati, M.; Orlando, T. Overhauser DNP in liquids on 13C nuclei. *eMagRes* **2019**, *8*, 11−18.
(39) Miao, Z.; Gonsales, S. A.; Ehm, C.; Mentink-Vigier, F.; Bowers, C. R.; Sumerlin, B. S.; Veige, A. S. Cyclic polyacetylene. *Nat. Chem.* **2021**, *13*, 792−799.
(40) Heeger, A. J.; Kivelson, S.; Schrieffer, J. R.; Su, W.-P. Solitons in conducting polymers. *Rev. Mod. Phys.* **1988**, *60*, 781−850.
(41) Goldberg, I. B.; Crowe, H. R.; Newman, P. R.; Heeger, A. J.; MacDiarmid, A. G. Electron spin resonance of polyacetylene and AsF5-doped polyacetylene. *J. Chem. Phys.* **1979**, *70*, 1132−1136.
(42) Kuroda, S.; Shirakawa, H. Electron-nuclear double-resonance evidence for the soliton wave function in polyacetylene. *Phys. Rev. B* **1987**, *35*, 9380−9382.
(43) Jeyadev, S.; Conwell, E. M. Soliton diffusion in trans-polyacetylene. *Phys. Rev. Lett.* **1987**, *58*, 258−261.
(44) Mehring, M.; Seidel, H.; Müller, W.; Wegner, G. Time resolved ESR of paramagnetic defects in undoped polyacetylene. *Solid State Commun.* **1983**, *45*, 1075−1077.
(45) Potje-Kamloth, K. In *Handbook of Surfaces and Interfaces of Materials*; Nalwa, H. S., Ed.: Academic Press, Burlington, 2001; pp 445−494.
(46) Overhauser, A. Polarization of Nuclei in Metals. *Phys. Rev.* **1953**, *92*, 411−415.
(47) Carver, T. R.; Slichter, C. P. Experimental Verification of the Overhauser Nuclear Polarization Effect. *Phys. Rev.* **1956**, *102*, 975−980.
(48) Can, T. V.; Caporini, M. a.; Mentink-Vigier, F.; Corzilius, B.; Walish, J. J.; Rosay, M.; Maas, W. E.; Baldus, M.; Vega, S.; Swager, T. M.; Griffin, R. G. Overhauser effects in insulating solids. *J. Chem. Phys.* **2014**, *141*, No. 064202.
(49) Wind, R. A.; Duijvestijn, M. J.; van der Lugt, C.; Manenschijn, A.; Vriend, J. Applications of dynamic nuclear polarization in 13C NMR in solids. *Prog. Nucl. Magn. Reson. Spectrosc.* **1985**, *17*, 33−67.
(50) Hovav, Y.; Feintuch, A.; Vega, S. Theoretical aspects of dynamic nuclear polarization in the solid state - the solid effect. *J. Magn. Reson.* **2010**, *207*, 176−89.
(51) Nechtschein, M.; Devreux, F.; Greene, R. L.; Clarke, T. C.; Street, G. B. One-Dimensional Spin Diffusion in Polyacetylene, CH_x. *Phys. Rev. Lett.* **1980**, *44*, 356−359.
(52) Völkel, G.; Dzuba, S. A.; Bartl, A.; Brunner, W.; Fröhner, J. Time-Resolved EPR on Polyacetylene. *physica status solidi (a)* **1984**, *85*, 257−263.
(53) Holczer, K.; Devreux, F.; Nechtschein, M.; Travers, J. P. Spin dynamics at low temperature in undoped trans-polyacetylene, (CH)x. *Solid State Commun.* **1981**, *39*, 881−884.
(54) Clark, W. G.; Glover, K.; Mozurkewich, G.; Murayama, C. T.; Sanny, J.; Etemad, S.; Maxfield, M. Electron Spin Motion in Trans-$(CH)_x$. *J. Phys. Colloq.* **1983**, *44* (C3), C3-239−C3-245.
(55) Pines, A.; Gibby, M. G.; Waugh, J. S. Proton-enhanced NMR of dilute spins in solids. *J. Chem. Phys.* **1973**, *59*, 569−590.

https://doi.org/10.1021/acs.jpclett.3c03591
J. Phys. Chem. Lett. 2024, 15, 3369−3375